



## ARTICLE

# The miracle role of lattice imperfections in benzene alkylation with methanol over mordenite

Hongfei Yun | Jiale Meng | Guixian Li | Peng Dong

College of Petrochemical Technology,  
Lanzhou University of Technology,  
Lanzhou, China

**Correspondence**

Guixian Li, College of Petrochemical  
Technology, Lanzhou University of  
Technology, Lanzhou 730050, China.  
Email: lgxwyf@163.com

**Funding information**

the Science and Technology Support  
Project of Gansu Province, Grant/Award  
Number: 1604GKCD026

**Abstract**

Mordenite (MOR) has demonstrated potential as a catalyst for alkylation due to high variability, intrinsic porosity, and outstanding stability. However, the contact probability of benzene and methanol has been limited by typical layered structures of MOR and there is no connection between layers. Here, we report the preparedness of H-MOR via a sequential post-treatment method based on a commercial MOR. H-MOR sample had appeared lattice imperfections inferred from characterization means. The samples were tested with benzene methylation reaction. Results show that the high conversion of benzene and the high selectivity of toluene were obtained from the miracle role of lattice imperfections in the H-MOR sample. Sequentially, based on the study of all catalyst structure and physical properties, a plausible reaction mechanism for the selectivity of the desired toluene was proposed.

**KEYWORDS**

benzene methylation, lattice imperfections, MOR, toluene

## 1 | INTRODUCTION

Hydrocarbon conversions catalyzed by acidic catalyst are a major class of reactions used for the wide number of industrial applications related to petrochemical, military industry, fine chemical, agriculture, and pharmaceuticals.<sup>[1–3]</sup> Here, we would introduce one of the brightest chemicals—toluene.

Toluene, an important chemical intermediate, is widely used for the production of fine chemicals from basic knowledge. Currently, the alkylation of benzene with methanol to produce toluene has attracted a lot of attention due to the decline of crude oil resources and the increase of demand for isocyanates.<sup>[4–7]</sup> Furthermore, because of the excessive production of benzene in petrochemical industry and the production overcapacity of methanol in coal chemical industry, it is imperative that the technology of benzene/methanol reaction to toluene

is systematically researched to further implement the coupling cycle development strategy of coal chemical industry and petrochemical industry.<sup>[8–10]</sup>

Generally, such reactions were carried out in the presence of homogeneous acid catalysts such as  $\text{AlCl}_3$ ,  $\text{ZnCl}_2$  in the presence of  $\text{HCl}$  or  $\text{H}_2\text{SO}_4$ .<sup>[11,12]</sup> Although the liquid acids were very effective for conversion, they also had drawbacks such as corrosion and difficulty in separation and recovery. Therefore, there had been many attempts to replace these homogenous catalysts with heterogeneous solid catalysts.<sup>[12,13]</sup>

In industry, zeolites catalysts were first introduced in oil-cracking, it was estimated that the higher gasoline yield resulting from the zeolite catalyst corresponded to an added value of 40 billion U.S. dollars/year.<sup>[14]</sup> The key point is that much of the success of zeolite catalysis can be attributed to the presence of micropores. However, in many cases, the sole presence of micropores can also be a

major limitation because mass transport to and from the active sites located within the micropores is slow, which is often limiting the performance of industrial catalysts. For benzene/methanol alkylation, general research was the preparation of p-xylene, but toluene as the ultimate product was a relatively difficult point and had been rarely reported.

To overcome this limitation, the synthesis of hierarchical zeolites with different framework types, such as ZSM-5,<sup>[15–22]</sup> Beta,<sup>[18,23]</sup> MWW,<sup>[24]</sup> X type,<sup>[25,26]</sup> and SSZ-13,<sup>[27]</sup> have been reported by means of several preparative methods. Of these, the synthesis of hierarchical mordenite (MOR) is of practical importance because MOR, with low preparative cost and strong acidity, has been used for catalytic reforming, alkylation, and isomerization processes in industry. On the other hand, large pore zeolites of the type MOR, Y, Beta, and MCM-22 do not exhibit p-selectivity, but are advantageously used in the synthesis of monoalkyl benzene (such as ethylbenzene and cumene).<sup>[15,28,29]</sup> So, we chose MOR as the catalyst of benzene alkylation with methanol.

The purpose of our study was to obtain a highly efficient catalyst for alkylation based on MOR. We prepared hierarchical MOR by using the post-treatment method based on a commercial MOR. The catalysts were characterized by using X-ray diffraction (XRD), N<sub>2</sub> adsorption/desorption, Fourier transform infrared absorption spectra (FT-IR), scanning electron microscope (SEM), and Temperature-Programmed Desorption (NH<sub>3</sub>-TPD). The performance of H-MOR catalyst in alkylation of benzene was deeply investigated. Furthermore, based on the discussion of the relationship between the structural properties and the catalytic performance, a plausible reaction mechanism for the selective formation of toluene was proposed.

## 2 | EXPERIMENTAL

### 2.1 | Materials

Commercial MOR, Benzene ( $\geq 99.5\%$ ), Methanol ( $\geq 99.5\%$ ), Methanoic acid (MA  $\geq 99.5\%$ ), Ammonium nitrate (AN  $\geq 99.5\%$ ), and Citric acid (CA  $\geq 99.5\%$ ) were purchased from the Catalyst Plant of Lanzhou (China). All commercial chemicals were used directly without further purifications.

### 2.2 | Preparation of catalysts

Commercial MOR was retreated by the high-temperature (823 K) processing for 4 hr, and then MOR was ion-

exchanged with a solution of 1 M MA at 353 K for 1 hr under stirring (repeated three times). Then filtered, washed with distilled water, and dried at 453 K. The dried sample was calcined in air at 823 K for 4 hr. The obtained sample was labeled H-MOR.

The catalysts were named on the basis of the concentration of MA used for the treatment of MOR, where H-MOR-1, H-MOR, and H-MOR-2 represent the MOR treated with 0.5 N, 1 N, and 1.5 N MA, respectively.

Other kinds of the catalyst were named on the basis of different kinds of modifiers used for the treatment of MOR, where H-MOR-AN and H-MOR-CA represent the MOR treated with AN and CA, respectively.

### 2.3 | Catalyst characterization

BET surface areas of reduced catalysts were measured by N<sub>2</sub> adsorption/desorption at 77 K using a Micromeritics ASAP 2010 instruments. Before measurement, the samples were degassed under vacuum at 130°C overnight.

XRD patterns of catalysts were obtained with a D/MAX-2400 X-ray diffractometer equipped with atmosphere and temperature control stages and using Cu-K $\alpha$  radiation ( $\lambda = 1.542 \text{ \AA}$ ) operated at 40 kV and 50 mA. In these experiments, XRD patterns were recorded every 50°C with a ramp rate of 10°C/min up to 700°C under 5% H<sub>2</sub>/N<sub>2</sub>.

FT-IR of the materials were acquired on a Nicolet Nexus 670 FT-IR spectrometer (Thermo Nicolet, USA) at room temperature in KBr pellets over the range of 7,400~350 cm<sup>-1</sup> under the atmospheric conditions.

NH<sub>3</sub>-TPD was performed by AutoChem2920 (Micromeritics) aiming to determine the nature of acids sites.

### 2.4 | Catalytic activity tests

Catalytic activity of the samples was measured in a continuous-flow jet bubbling reactor with a glass tube (8 mm i.d.) at atmospheric pressure. The catalyst (0.5 g) was heat-treated in situ from environmental temperature to 673 K at 10 K/min. Then benzene/methanol mixture (1:1) was fed into the reactor (WHSV = 2.0 hr<sup>-1</sup>).

## 3 | RESULTS AND DISCUSSION

### 3.1 | Catalyst characterizations

Figure 1 shows the XRD patterns of MOR and H-MOR catalysts. All the samples exhibited the typical

characteristic patterns with peaks observed at  $2\theta$  of  $6.50^\circ$ ,  $8.60^\circ$ ,  $9.76^\circ$ ,  $13.44^\circ$ ,  $13.82^\circ$ ,  $22.18^\circ$ ,  $25.60^\circ$ , and  $27.66^\circ$ , which corresponded to the structure of MOR topology in comparison with standard MOR from Database of Zeolite Structures. The broadening of the observed peak indicated the nanoscale character of MOR and H-MOR samples.<sup>[30]</sup> Notably, the crystallinity of H-MOR showed a slight decrease from that of MOR, which meant that dealumination had a minor influence on the crystallinity of MOR. Compared with standard MOR from Database of Zeolite Structures, 12 member-rings (12-MR) (110) was

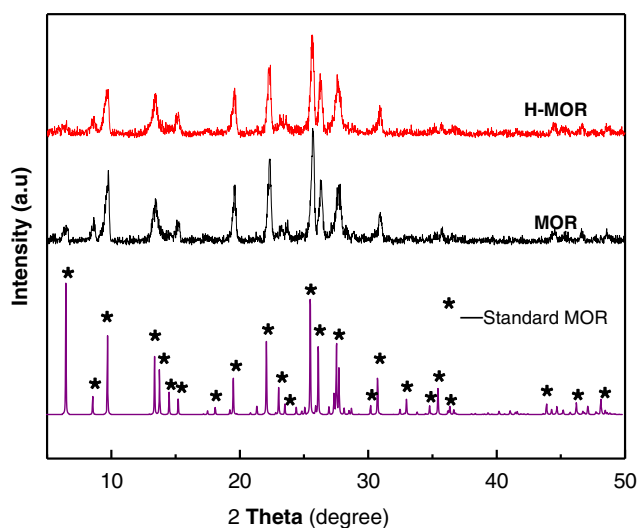


FIGURE 1 XRD patterns of MOR and H-MOR

decreased greatly in Figure 1.<sup>[31]</sup> The results show that 110 crystal plane (12-MR) has been damaged or cut off, where the defect of the surface structure was increased, the strain was produced, and the peak area was decreased. These results are in accordance with the phenomenon of SEM in Figure 2.

SEM images of all the samples are shown in Figure 2. Obviously, the MOR sample was typically layered structures and stack together (length of about approximately  $1\ \mu\text{m}$ ) (Figure 2a). In comparison, for H-MOR samples, the crystal shape becomes similar to round and crystal size was about a third of MOR. The results show that the crystal structure has been deformed, which was attributed to decrease greatly of 12-ring in Figure 1. Straight cylindrical pores were distorted or disconnected to some extent and each layer was not overlapping with each other because there is a certain displacement. Therefore, the average diameter may be reduced from  $0.66$  to  $0.4\ \text{nm}$ .<sup>[32]</sup> These results indicated that the process of post-treatment had an effect on the particle size and morphology of MOR. These results are in accordance with the results from XRD.

Nitrogen sorption isotherms are shown in Figure 3. Both MOR and H-MOR exhibited type IV nitrogen sorption isotherms typical of zeolites,<sup>[8]</sup> which was typical for a porous material with a mesoporous structure. The textural properties of samples are listed in Table 1, which compares the surface area and pore volume of MOR and H-MOR samples. Compared with the original MOR, H-MOR samples showed a slight increase in the pore

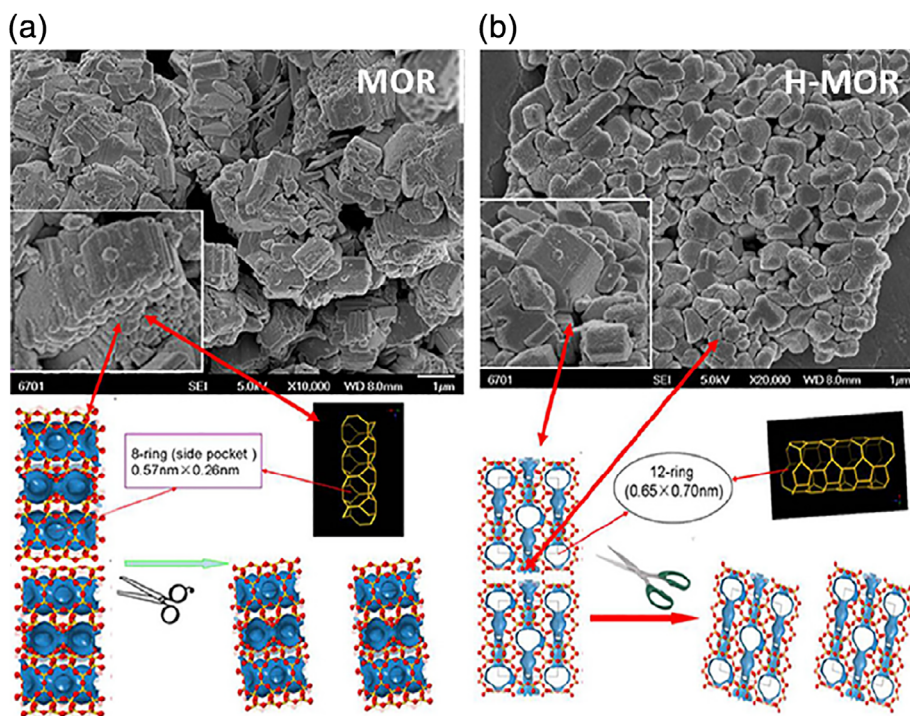


FIGURE 2 SEM images of MOR (a) and H-MOR (b)

volume ( $V_{\text{Micro}}$ ) of the micropores. For H-MOR, the micropores are filled at a relative pressure of  $<0.1$ . However, for conventional MOR, the mesopores are filled at total relative pressure range showing a large number of mesopores present in these MOR materials, as evidenced by the uptake of  $N_2$ .

The FTIR transmittance patterns of the samples also indicated that zeolite structure was basically protected during acid treatment (Figure 4), which shows the FTIR spectra ranging from 400 to 4,000  $\text{cm}^{-1}$  of MOR and H-MOR or the comparison and explanation of MOR and H-MOR samples about FTIR spectra are shown in Table 2.

Skeleton changes of MOR and MOR treated by MA are no significant change, where are mainly the vibration strength of skeleton. In contrast, the main band ( $1,070 \text{ cm}^{-1}$ ) is slightly shifted to the high band ( $1,080 \text{ cm}^{-1}$ ), the band narrow, and intensity increases (Figure 4b), which are caused by the treated MA bringing about decreasing of Al. As is well-known, the length of the Si-OH ( $0.161 \text{ nm}$ ) is less than Al-OH ( $0.175 \text{ nm}$ ), which changes the structure parameters of MOR. According to Man Li, etc.<sup>[35]</sup>:

1. The silicon atoms are more electronegative than aluminum atoms in the tetrahedron of Si-Al-O.
2. The length of the Si-OH groups is less than Al-OH groups.

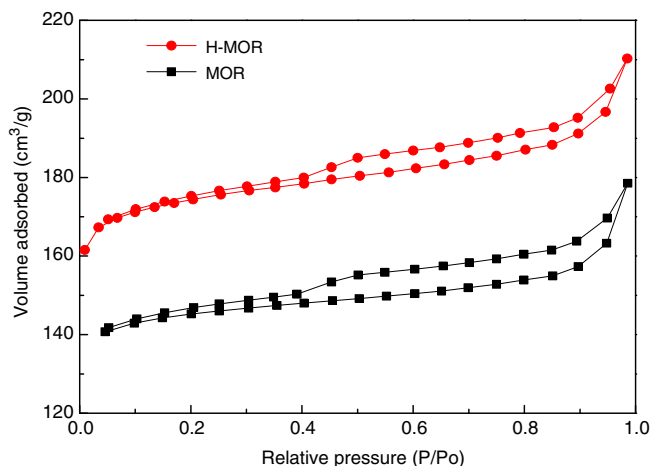


**FIGURE 3** Nitrogen adsorption/desorption isotherm of MOR and H-MOR samples

Therefore, the Al atoms of H-MOR are gradually removed, which result in the increase of the force constant, so the (Si, Al)-OH groups are shifted to the high bands. Meanwhile, the intensity of the (Si, Al)-OH tetrahedron at  $803\text{--}1326 \text{ cm}^{-1}$ , the stretching vibration of -OH groups at  $1,630 \text{ cm}^{-1}$  and  $3,470 \text{ cm}^{-1}$  to H-MOR is increased for the above reasons. In conclusion, the above analysis shows that the skeletal structure of MOR has not changed much after the process of MA treatment and Al is decreased.

The acidity of the samples is measured by (TPD) of  $\text{NH}_3$ , where the samples exhibited a two-peak pattern; the one located below  $250^\circ\text{C}$  correlated to the weak acid sites and the second peak situated above  $300^\circ\text{C}$  correlation to strong acid sites (Figure 5).<sup>[1]</sup>

The strong acid strength to an extent was increased and reduced the weak acid to an extent using MA treatment, but the acid amount was not increased. Therefore, compared with MOR, H-MOR had a lower weak acid strength and more strong acid sites, which are associated with the degree of further alkylation.

Figure 6 shows Py-IR spectra of these catalysts at a specific temperature. The spectra of these samples exhibit four bands at frequencies  $1,540$ ,  $1,490$ , and  $1,450 \text{ cm}^{-1}$ . Bands at  $1,450 \text{ cm}^{-1}$  indicate the presence of coordinated pyridine of the Lewis acid sites of the catalyst. IR band appearing at  $1,490 \text{ cm}^{-1}$  is associated with the vibration of the pyridine ring on Brönsted

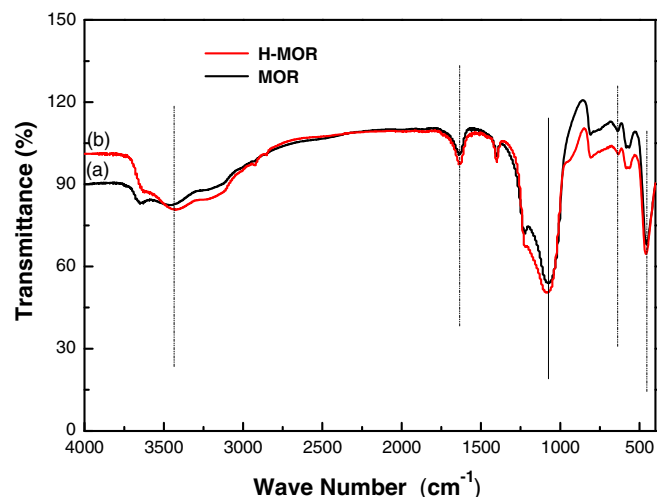


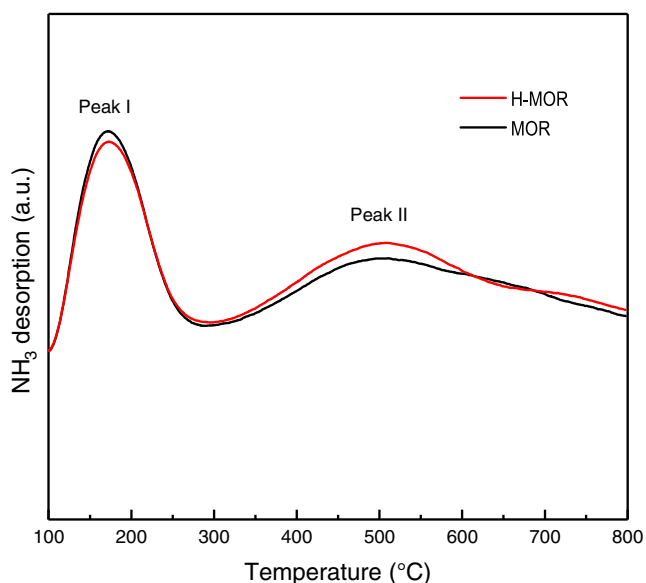
**FIGURE 4** FT-IR spectra of MOR and H-MOR samples

**TABLE 1** Physicochemical properties of MOR and H-MOR samples

Sample	$S_{\text{BET}}/(\text{m}^2 \text{ g}^{-1})$	$V_{\text{total}}/(\text{cm}^3 \text{ g}^{-1})$	$V_{\text{meso}}/(\text{cm}^3 \text{ g}^{-1})$	$V_{\text{micro}}/(\text{cm}^3 \text{ g}^{-1})$	Average pore diameter/nm
MOR	387	0.25	0.05	0.20	2.58
H-MOR	466	0.26	0.04	0.21	2.25

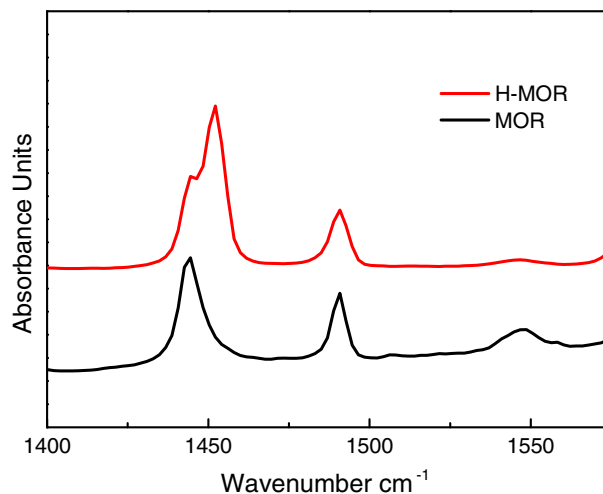
**TABLE 2** Comparison and explanation of MOR and H-MOR samples about FT-IR spectra

Construction unit	Wave number/cm <sup>-1</sup>		Changing situation		Remarks
	MOR	H-MOR	Shifted	Peak shape changed	References
(Si, Al)-OH tetrahedron	457	457	No	No	[33,34]
5MR	540–620	540–620	No	No	
(Si, Al)-OH tetrahedron	1,070	1,080	Slightly shifted to the high band	The band narrow and intensity increases	[34,35]
	803–1,326	803–1,273			
Stretching vibration of -OH groups	1,630	1,630	No	Intensity increases	[34]
	3,470	3,470	No	Intensity increases	[34]

**FIGURE 5** Acid strength distribution of MOR and H-MOR samples measured by NH<sub>3</sub>-TPD

and Lewis acid sites. In addition, IR band nearly 1,540 cm<sup>-1</sup> are due to the adsorption of pyridine coordinated on Brönsted acid sites.<sup>[22,36,37]</sup> However, the results show that the peak of B acid at 1,540 cm<sup>-1</sup> was reduced and the peak at 1,450 cm<sup>-1</sup> shifted to the high wave, which might be because of the removal of Al. At the same time, it was shown that the lattice defects of H-MOR resulted from the modification, which was beneficial to the migration of the reactants in the pore channels of H-MOR and enhanced the probability of approaching the active sites.<sup>[38]</sup>

From the research above, we concluded that acid treatment did not only improve the pore accessibility but also further adjusted the acid properties of MOR. H-MOR catalyst would help to increase efficiently the conversion of benzene and the selectivity of toluene. The results were interesting and lead to further scientific work.

**FIGURE 6** IR spectra of the samples after pyridine desorption

### 3.2 | Catalytic activity

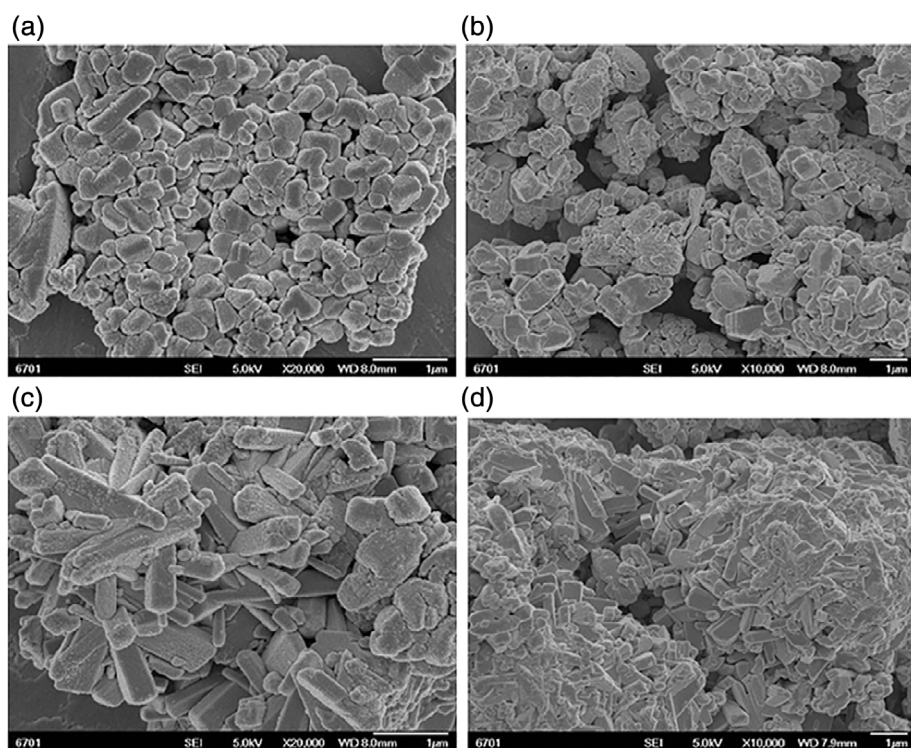
The catalytic test of MOR, H-MOR, H-MOR-1, H-MOR-2, H-MOR-AN, and H-MOR-CA catalysts is presented in Table 3. Toluene and xylene were found to be the predominant products after alkylation, but a significant difference was shown. The best result especially toluene was found to be the predominant products over the H-MOR catalyst. Other byproducts such as ethylbenzene, tri-methylbenzene, coke, etc. are also detected in small amounts (sel. % = 4.1–5.7%) except for the H-MOR-AN catalyst (11.7%).

Obviously, MOR exhibited a low catalytic activity, with benzene conversion of 34.0% and toluene selectivity of 80.9%. Interestingly, H-MOR gave much higher catalytic activity than MOR. The benzene conversion reached 48.4% and toluene selectivity of 90.3%, even a little better than that of H-MOR-1 (0.5 mol/L, 41.3% and 84.4%) and H-MOR-2 (1.5 mol/L, 45.4% and 86.7%). These differences might be due to different concentration of MA, which would lead to the changes

**TABLE 3** Products content of benzene alkylation with methanol over the different catalysts

Catalysts	Benzene conversion/%	Product selectivity/%			
		Toluene	Xylene	Toluene + Xylene	Others
MOR	34.0	80.9	12.9	94.8	6.2
H-MOR	48.4	90.3	5.6	95.9	4.1
H-MOR-1	41.3	84.4	10.2	94.6	5.4
H-MOR-2	45.4	86.7	8.6	95.3	5.7
H-MOR-AN	34.8	72.9	15.4	88.3	11.7
H-MOR-CA	48.3	81.0	14.4	95.4	4.6

Note: Reaction optimum condition: Catalyst = 0.5 g, T = 400°C, Reaction time = 3 hr, Pressure = normal atmosphere, WHSV = 2.0 hr<sup>-1</sup>, Feed (Benzene/Methanol) ratio = 1:1.

**FIGURE 7** SEM images of H-MOR (a, 1 mol/L), H-MOR-2 (b, 1.5 mol/L), H-MOR-AN (c, 1 mol/L), and H-MOR-CA (d, 1 mol/L)

of physicochemical properties (Figure 7) for the catalyst and reduce the yield of toluene. Notably, the difference was: as showed in Figure 7b,d of the crystals of H-MOR-2, H-MOR-CA exhibited more disorderly shape with rough surfaces and even the phenomenon of agglomeration. This morphology arose from modified agent to bring about more dealumination, which led to collapse of catalyst tunnel, even agglomerate. For H-MOR-AN, the crystal shape became similar to round and crystal size was not changed in Figure 7c. These results indicated that the different acid concentrations (Figure 8) and different acids had an effect on the particle size and morphology of MOR.

### 3.3 | Mechanism of catalytic reaction

To sum up, the reaction was initiated on acid sites where protons on zeolites attacked benzene to form protonated benzene and methanol was activated by acid sites to generate  $\text{CH}_3^+\text{OH}^-$ , then protonated benzene and activated  $\text{CH}_3^+\text{OH}^-$  generate toluene. Deprotonation regenerated the sites to its original state. Toluene could be alkylated further forming xylene or tri-benzenes via a similar mechanism after sequential methylations as suggested by the reaction network in Figure 9. The source of carbon production had been evaluated by testing with only methanol, only benzene, or benzene/methanol (1:1) as raw material. Results show that the carbon production

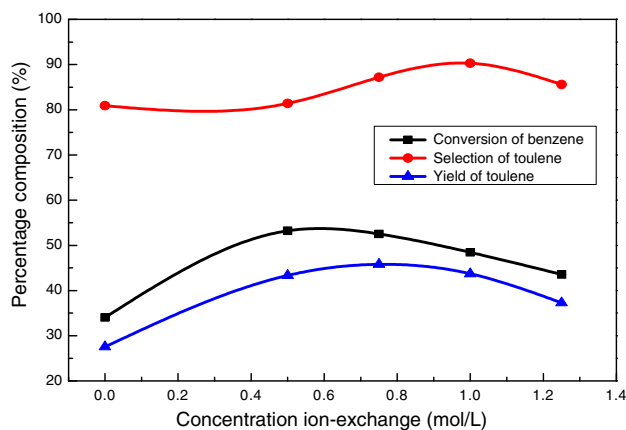


**FIGURE 8** Effects of different concentrations on catalytic activity

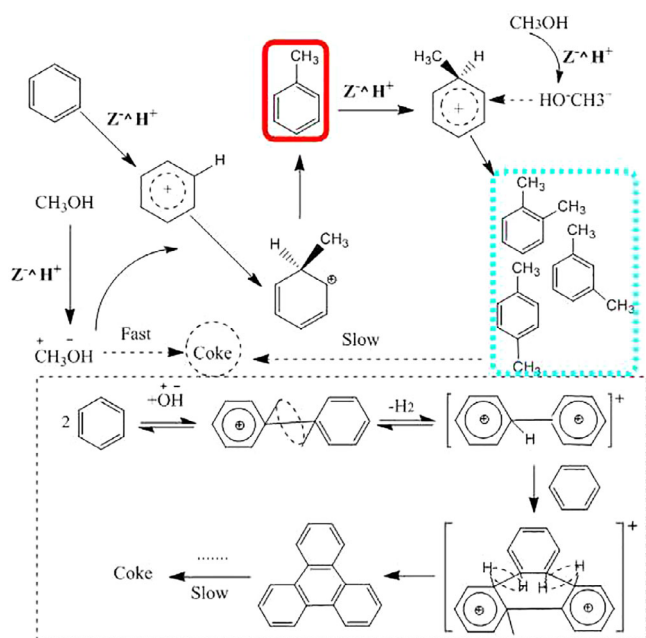


**FIGURE 9** Reaction network of benzene methylation and related products

rate of only methanol as a reactant was much higher than that of only benzene. The former was equivalent to that of benzene/methanol.

The reasons for the high conversion of benzene and the high selectivity of toluene were analyzed as follows by optimized geometries in Figure 10.

1. The acidity of the catalyst: more strong acid sites were associated with the high conversion of benzene.
2. Lattice Imperfections: Firstly, the crystal shape of the H-MOR sample became similar to round and crystal size diminished about a third of MOR in Figures 2 and 10, which was conducive to the

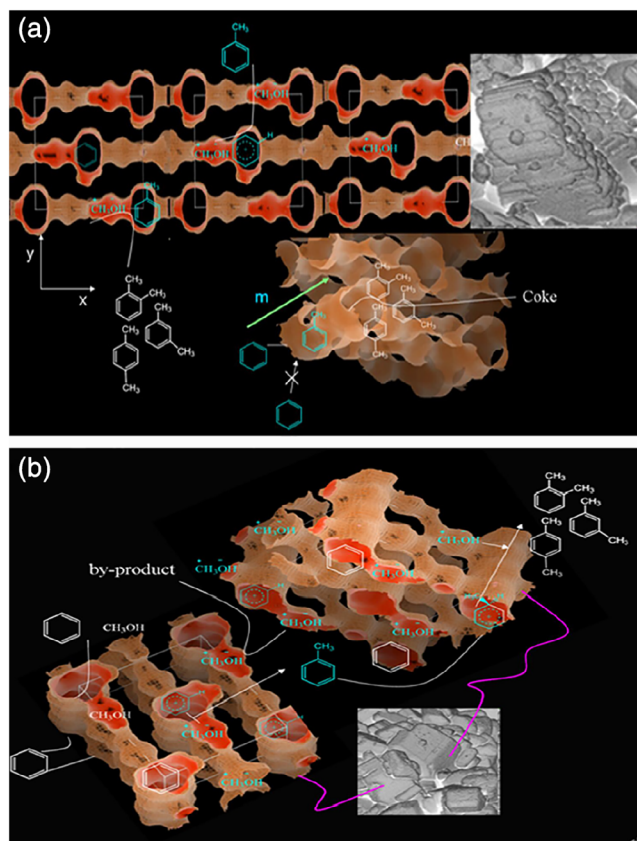


**FIGURE 10** Optimized geometries of benzene methylation over MOR (a) and H-MOR (b) catalysts. White-unactivated or byproduct, blue-activated or target product

rational use of space. The residence time of benzene in a microreactor was increased because straight cylindrical pores were distorted or disconnected to some extent and each layer was not overlapping with each other. Secondly, a lot of  $-\text{OH}$  in the 8-MR was exposed and the activation of  $\text{CH}_3^+$  in the 8-MR was much better than in the 12-MR. Third Point, because the channel of the catalyst becomes short, the update rate of benzene in the system was accelerated. Finally, the  $y$  direction was not connected in Figure 10a, which greatly reduces the contact probability of benzene and methanol. Therefore, these factors would enhance the conversion of benzene. Similarly, there was a long porous channel in the MOR in the  $m$  direction of Figure 10a, where the chance of both further react of toluene with  $\text{CH}_3^+$  and the side reaction of methanol were greatly increased, resulting in the selectivity of toluene being decreased.

3. Other research materials: Large pore zeolites of the type MOR, Y, Beta and MCM-22 were advantageously used in the synthesis of mono-alkyl benzene.<sup>[15,28,29,39,40]</sup>

## 4 | CONCLUSIONS

In our research, MOR catalysts with different concentrations of MA and other modifier were investigated in the alkylation of benzene with methanol. The experiment result shows that the high conversion of benzene (48.4%) and the selectivity of the desired toluene (90.3%) were mainly controlled by lattice imperfections and external acid sites that were affected by dealumination degree of the H-MOR catalyst. Based on literature investigation, catalyst characterization, and catalytic activity tests, results show that the H-MOR catalyst is of great importance for potential industrial application.

### ACKNOWLEDGMENTS

We acknowledge financial support from the Science and Technology Support Project of Gansu Province (1604GKCD026).

### CONFLICT OF INTEREST

The authors declare no conflicts of interest.

### REFERENCES

- [1] S. K. Saxena, N. Viswanadham, *Appl. Surf. Sci.* **2017**, 392, 384.
- [2] A. Feller, J. A. Lercher, *Adv. Catal.* **2004**, 48, 229.
- [3] S. L. You, Q. Cai, M. Zeng, *Soc. Rev.* **2009**, 38, 2190.
- [4] Y. P. Wijaya, I. Kristianto, H. Lee, J. Jae, *Fuel* **2016**, 182, 588.
- [5] Z. Lin, V. Nikolakis, M. Ierapetritou, *Ind. Eng. Chem. Res.* **2014**, 53, 10688–99.
- [6] Q. Zhang, J. Tan, T. Wang, Q. Zhang, L. Ma, S. Qiu, Y. Weng, *Fuel* **2016**, 165, 152.
- [7] L. Wang, H. Lei, Q. Bu, S. Ren, Y. Wei, L. Zhu, X. Zhang, Y. Liu, G. Yadavalli, J. Lee, S. Chen, J. Tang, *Fuel* **2014**, 129, 78.
- [8] H. L. Hu, Q. F. Zhang, J. Cen, X. N. Li, *Catal. Lett.* **2015**, 145, 715.
- [9] M. P. M. Nicolau, P. S. Barcia, J. M. Gallegos, et al., *J. Phys. Chem. C* **2009**, 113, 13173–13179.
- [10] F. Schmidt, C. Hoffmann, F. Giordanino, S. Bordiga, P. Simon, W. Carrillo-Cabrera, S. Kaskel, *J. Catal.* **2013**, 307, 238.
- [11] K. Y. Leng, Y. Wang, C. M. Hou, C. Lancelot, C. Lamonier, A. Rives, Y. Y. Sun, *J. Catal.* **2013**, 306, 100.
- [12] I. Iovel, K. Mertins, J. Kischel, A. Zapf, M. Beller, *Angew. Chem. Int. Ed.* **2005**, 44, 3913.
- [13] J. J. Chiu, D. J. Pine, S. T. Bishop, B. F. Chmelka, *J. Catal.* **2004**, 221, 400.
- [14] C. H. Christensen, K. Johannsen, I. Schmidt, C. H. Christensen, *J. Am. Chem. Soc.* **2003**, 125, 13370–13371.
- [15] T. Odedairo, S. Al-Khattaf, *Catal. Today* **2013**, 204, 73.
- [16] D. Van Vu, M. Miyamoto, N. Nishiyama, Y. Egashira, K. Ueyama, *J. Catal.* **2006**, 243, 389.
- [17] Z. H. Wen, D. Q. Yang, X. He, Y. S. Li, X. D. Zhu, *J. Mol. Catal. A-Chem.* **2016**, 424, 351.
- [18] J. V. Mynsbrugge, M. Visur, U. Olsbye, P. Beato, M. Bjørgen, V. V. Speybroeck, S. Svelle, *J. Catal.* **2012**, 292, 201.
- [19] H. L. Hu, Q. F. Zhang, J. Cen, X. N. Li, *Catal. Commun.* **2014**, 57, 129.
- [20] H. L. Jin, M. B. Ansari, E. Y. Jeong, S. E. Park, *J. Catal.* **2012**, 291, 55.
- [21] K. Y. Wang, X. S. Wang, *Micropo. Mesopo. Mater.* **2008**, 112, 187.
- [22] H. L. Hu, J. H. Lyu, Q. T. Wang, Q. F. Zhang, J. Cen, X. N. Li, *RSC Adv.* **2015**, 5, 32679.
- [23] S. Saepurahman, M. Visur, U. Olsbye, M. Bjørgen, S. Svelle, *Top Catal.* **2011**, 54, 1293.
- [24] S. Inagaki, K. Kamino, E. Kikuchi, M. Matsukata, *Appl. Catal. A-Gen* **2007**, 318, 22.
- [25] B. B. Tope, W. O. Alabi, A. M. Aitani, H. Hattori, S. S. Al-Khattaf, *Appl. Catal. A-Gen.* **2012**, 443–444, 214.
- [26] J. Jiang, G. Z. Lu, C. X. Miao, X. Wu, W. H. Wu, Q. Sun, *Micropo. Mesopo. Mater.* **2013**, 167, 13.
- [27] L. Wu, V. Degirmenci, P. Magusin, N. Lousberg, E. Hensen, *J. Catal.* **2013**, 298, 27.
- [28] B. Wichterlova, J. Cejka, N. Zilkova, *Microporous Materials* **1996**, 6, 405.
- [29] K. J. A. Raj, E. J. P. Malar, V. R. Vijayaraghavan, *J. Mol. Catal.* **2006**, 243, 99.
- [30] Q. M. Sun, Y. H. Ma, N. Wang, X. Li, D. Y. Xi, J. Xu, F. Deng, K. B. Yoon, P. Oleynikov, O. Terasaki, J. H. Yu, *J. Mater. Chem. A* **2014**, 2, 17828.
- [31] H. Hattori, Y. Ono, *Solid acid catalysis*, Fudan University Press, China **2016**, p. 90.
- [32] P. B. Venuto, P. S. Landis, *Organic catalysis over crystalline Aluminosilicates*, Petroleum Chemical Press, New Jersey, **1968**, p. 2.
- [33] K. H. Lee, B. H. Ha, *Micropo. Mesopo. Mater.* **1998**, 23, 211.
- [34] X. Y. Wang, *Catalyst characterization*, East China University of Science and Technology Press, China **2008**, p. 139.
- [35] H. L. Zhang, M. J. Zhang, H. W. Li, Y. J. Chou, Y. Chen, *J. Wuhan Uni. Sci. Tech* **2001**, 24, 361.
- [36] F. Wang, X. L. Xu, K. P. Sun, *React. Kinet. Catal. Lett.* **2008**, 93, 135.
- [37] L. Jaehong, L. S. Seong, Y. Y. Jackie, *Chem. Commun.* **2010**, 46, 806.
- [38] Y. Z. Zhang, G. L. Yin, S. J. Gu, *Chinese J. Catal.* **1986**, 7, 40.
- [39] T. Yashima, H. Ahmad, K. Yamazoki, M. Katsuata, N. Hara, *J. Catal.* **1970**, 16, 273.
- [40] T. Yashima, K. Yamazoki, H. Ahmad, M. Katsuata, N. Hara, *J. Catal.* **1970**, 17, 151.

**How to cite this article:** Yun H, Meng J, Li G, Dong P. The miracle role of lattice imperfections in benzene alkylation with methanol over mordenite. *J Chin Chem Soc.* 2020;1–8. <https://doi.org/10.1002/jccs.201900412>